1	
2	
3	
4	Local interactions underlying collective motion
5	in human crowds
6	
7	
8	Kevin W. Rio
9	Gregory C. Dachner
10	William H. Warren*
11	
12	
13	Department of Cognitive, Linguistic and Psychological Sciences
14	Brown University
15	Providence, RI, 02912, USA
16	
17	*Corresponding author: <u>Bill_Warren@brown.edu</u>
18	+1 401 863 3980 (office)
19	+1 401 863 2255 (fax)
20	
21	
22	RUNNING HEAD: Collective crowd motion

Abstract

23

24

25

26

27

28

29

30

31

32

33

34

35

36

37

It is commonly believed that global patterns of motion in flocks, schools, and crowds emerge from local interactions between individuals, through a process of self-organization. The key to explaining such collective behavior thus lies in deciphering these local interactions. We take an experiment-driven approach to modelling collective motion in human crowds. Previously, we observed that a pedestrian aligns their velocity vector (speed and heading direction) with that of a neighbor. Here we investigate the neighborhood of interaction in a crowd: which neighbors influence a pedestrian's behavior, how this depends on neighbor position, and how the influences of multiple neighbors are combined. In three experiments, a participant walked in a virtual crowd whose speed and heading were manipulated. We find that neighbor influence is linearly combined and decreases with distance, but not with lateral position (eccentricity). We model the neighborhood as (a) a circularly symmetric region with (b) a weighted average of neighbors, (c) a uni-directional influence, and (d) weights that decay exponentially to zero by 5m. The model reproduces the experimental data and predicts individual trajectories in observational data on a human 'swarm'. The results yield the first bottom-up model of collective crowd motion.

38

39

Keywords

- 40 Collective behavior, crowd dynamics, pedestrian dynamics, flocking, agent-based model, self-
- organization 41

Rio, Dachner, & Warren

Background

Striking displays of collective motion are observed in a variety of species, from flocks of
starlings and schools of herring to crowds of pedestrians in public spaces (Helbing, Buzna,
Johansson, & Werner, 2005; Vicsek & Zafeiris, 2012). Under certain conditions, groups of
individuals coordinate their speed and heading (direction of travel) to yield patterns of coherent
motion. A better understanding of the dynamics of human crowds is of particular importance
considering the incidence of casualties in stampedes and emergency evacuations (Hsieh, Ngai,
Burkle, & Hsu, 2009).
It is commonly believed that global patterns of collective behavior emerge from local
interactions between individuals in a process of self-organization (Couzin & Krause, 2003;
Haken, 1983; Sumpter, 2006). The key to explaining collective motion thus lies in
characterizing these local interactions and how they give rise to global patterns. Numerous
mathematical and computational models have been proposed within this local-to-global
framework (Sumpter, Mann, & Perna, 2012). These 'microscopic' models describe behavioral
'rules' that govern an individual's interactions with neighbors, as well as other entities such as
goals and obstacles. In particular, they assume that an individual is influenced by multiple
neighbors in a zone of influence, or neighborhood of interaction. Once local rules are
formalized, agent-based simulations are used to test whether the model reproduces characteristic
patterns of collective motion and, ideally, to predict behavior in novel situations.
Such microscopic models have proliferated in recent years. Early models of fish schooling
led to the dominant attraction-repulsion approach (Reynolds, 1987; Schellinck & White, 2011).
This class of models is predicated on three basic rules, (a) attraction: move toward neighbors in
a far zone. (b) repulsion: move away from neighbors in a near zone, and (c) alignment: match

Rio, Dachner, & Warren

the velocity (speed and heading) of neighbors in an intermediate zone. Couzin, Krause, James, Ruxton, and Franks (2002) showed that, by adjusting parameters for the radii of alignment and attraction zones, such a model can generate qualitatively distinct patterns, including unaligned aggregation (shoaling), strongly aligned translational motion (schooling), and coherent rotational motion (mills).

The self-propelled particle model (Czirók & Vicsek, 2000) assumed only a minimal alignment rule, in which each individual adopts the mean heading direction of all neighbors within a zone of fixed radius. This rule alone can generate coherent translational motion

(Vicsek, Czirók, Ben-Jacob, Cohen, & Shochet, 1995). Conversely, the influential social force

model (Helbing & Molnár, 1995) eschews an alignment term, such that collective motion

emerges from position-based attraction and repulsion forces. This, too, generates plausible

global patterns, but local trajectories tend to resemble particle motion more than human

locomotion (Pelechano, Allbeck, & Badler, 2007).

Recently, 'cognitive heuristic' or 'vision-based' models have been proposed (Moussaïd, Helbing, & Theraulaz, 2011; Ondrej, Pettré, Olivier, & Donikian, 2010), which employ simple rules based on the distance or time-to-contact with objects to steer toward the goal while avoiding collisions. Although we are sympathetic with this approach, behavioral experiments are necessary to justify the proposed heuristics.

There is thus a plethora of theoretical models of collective motion. With recent advances in motion tracking of bird flocks and human crowds, they are beginning to be compared against empirical data (Ballerini et al., 2008; Helbing et al., 2005; Hildenbrandt, Carere, & Hemelrijk, 2010; Lukeman, Li, & Edelstein-Keshet, 2010; Moussaïd et al., 2012). However, successfully

¹ 'Alignment' is often used to refer to the orientation of the body's longitudinal axis, which typically corresponds with the velocity vector.

Rio, Dachner, & Warren

simulating observational data is insufficient to confirm a model, for different local rules can give rise to the same motion patterns (Vicsek & Zafeiris, 2012; Weitz et al., 2012). To decipher the local rules, experimental manipulation at the level of individual behavior is necessary (Gautrais et al., 2012; Sumpter et al., 2012).

We have been pursuing such an experiment-driven, bottom-up approach, called *behavioral dynamics* (Warren, 2006; Warren & Fajen, 2008), with the aim of building a pedestrian model that can explain emergent behavior. Elementary locomotor behaviors are studied individually and modeled with simple attractor/repeller dynamics; these models are analogous to behavioral 'rules' but emphasize their dynamical rather than logical form. Related experiments identify *visual control laws*, incorporating the optical information that regulates each behavior. The resulting pedestrian model has five components: (a) steering to a goal, (b) obstacle avoidance, (c) moving target interception, (d) moving obstacle avoidance, and (e) braking to avoid collision, analogous to a local 'repulsion' rule (Fajen & Warren, 2003, 2007; Warren & Fajen, 2008). Linearly combining these components successfully predicts trajectories in more complex environments (Bonneaud & Warren, 2014; Warren & Fajen, 2008).

To understand the basis of collective motion, we recently studied binary pedestrian following. We found that a pedestrian p aligns with a neighbor n directly ahead (the leader) by accelerating to match the leader's speed (\dot{r}) and heading direction (ϕ) (Dachner & Warren, 2014; Lemercier et al., 2012; Rio, Rhea, & Warren, 2014). These results allowed us to specify a simple model of the alignment dynamics for binary interactions:

$$\ddot{r}_p = c(\dot{r}_n - \dot{r}_p) \tag{1}$$

$$\ddot{\phi}_p = -k\sin(\phi_n - \phi_p) \tag{2}$$

where \ddot{r} , ϕ are linear and angular acceleration, and c , k are gain parameters that depend on the
leader's distance. To explain collective motion, however, requires determining how a pedestrian
is influenced by multiple neighbors.

The present paper thus aims to characterize the neighborhood of interaction underlying collective motion in human crowds. In particular, we ask which neighbors visually influence a pedestrian's behavior (i.e. are *visually coupled*), how the degree of influence (*coupling strength*) depends on neighbor position, and how the influences of multiple neighbors are combined.

We experimentally test three hypotheses about the neighborhood of interaction. (1)
Superposition hypothesis. Most models of collective motion assume that binary interactions
between a pedestrian and each neighbor are linearly combined. That is, the response of a
pedestrian in a crowd is the combination of individual responses to each neighbor, a property
known as superposition. This hypothesis predicts that as more neighbors change direction or
speed, the pedestrian's response should increase proportionally. (2) Distance hypothesis. Many
models assume a constant coupling strength within an alignment zone with 'hard' boundaries
(Couzin et al., 2002; Czirók & Vicsek, 2000; Reynolds, 1987; Schellinck & White, 2011).
However, Fajen and Warren (2003) found that attraction or repulsion strength decreases
exponentially with the distance of a goal or obstacle, leading us to expect that the coupling
strength for alignment will also decay with distance. (3) Eccentricity hypothesis. There are
numerous reports of an elliptical 'personal space' for walking pedestrians (Fajen & Warren,
2003; Gérin-Lajoie, Richards, & McFadyen, 2005; Helbing & Molnár, 1995). This implies that,
for a given distance, coupling strength should decrease with a neighbor's lateral position or

Rio, Dachner, & Warren

eccentricity, the horizontal angle from the current heading direction.² Neighbors directly ahead should exert the greatest influence, while the influence of those to the left and right should decrease symmetrically to the edges of the field of view.

The results reveal that a pedestrian is strongly coupled to neighbors within a local neighborhood, that their influence is linearly combined, consistent with the superposition hypothesis, and that coupling strength decreases exponentially with distance out to 4-5m, consistent with the distance hypothesis. In contrast, we find little evidence that coupling strength depends on eccentricity within the field of view. The results enable us to specify a model of the local neighborhood that reproduces the experimental data and predicts individual trajectories in motion-capture data on a human 'swarm'. We thus formulate the first bottom-up model of collective motion in human crowds, providing a basis for realistic models of crowd dynamics.

Experiments: Walking with a virtual crowd

To probe the visual coupling between a pedestrian and their neighbors experimentally, we created a novel paradigm in which a human participant actively walks with a virtual crowd. This allowed us to manipulate the behavior of virtual neighbors and measure their influence on the participant's trajectory. To determine the alignment response, we suddenly changed (perturbed) the heading direction or walking speed of a subset (S) of the virtual neighbors (N), and recorded the participant's adjustment in lateral position or walking speed.

Experiment 1 tested the superposition hypothesis by varying the number of neighbors in the perturbed subset; Experiment 2 tested the distance hypothesis by selectively perturbing

² We assume the body midline and field of view are typically aligned with the heading direction (see Figure 4b).

neighbors in a near zone and/or a far zone; and Experiment 3 tested the eccentricity hypothesis by varying the lateral position of the perturbed neighbors.

Experimental Methods

Participants

Separate groups of ten volunteers participated in Experiment 1 (5F, 5M), Experiment 2 (6F, 4M), and Experiment 3 (6F, 4M). Participants were recruited through announcements posted on the Brown University campus. None reported any visual or motor impairment.

Apparatus

The experiments were conducted in the Virtual Environment Navigation Laboratory (VENLab) at Brown University. Participants walked in a 12x14m tracking area while wearing a stereoscopic head-mounted display (HMD, Oculus Rift DK1, 640x800 pixels per eye, 90°H x 65°V field of view, 60 Hz frame rate). Head position and orientation were recorded with an ultrasonic/inertial tracking system (Intersense IS-900, 60 Hz sampling rate) and used to update the display (50-67ms latency).

Displays

The virtual environment consisted of a granite-textured ground plane with a green start pole and a red orienting pole (3m high, 0.2m radius, 12.7m apart) and blue sky. The virtual crowd was generated using 3D human models (WorldViz Complete Characters) (Figure 1a), animated with a walking gait at a randomly varied phase. Thirty virtual humans were positioned on two circles (radius 1.5m, 3.5m) with the participant at the center (Figure 1b) to enhance the sense of immersion. Twelve of them (N=12) were experimentally manipulated, and appeared on two 90°

Rio, Dachner, & Warren

arcs centered on the initial walking direction, within the typical field of view. Five of these neighbors were placed at equal intervals on the 1.5m radius arc (near zone), and seven on the 3.5m radius arc (far zone); their positions were then subjected to Gaussian jitter in polar coordinates (distance Δr : SD=0.15m; eccentricity $\Delta \theta$: SD=8°). The remaining 18 were also placed at equal intervals and similarly jittered. A different configuration was generated for each trial; all participants received the same set of configurations, but virtual humans were randomly assigned to the positions.

During a trial, all virtual humans accelerated from a standstill (0 m/s) to a speed of 1.3 m/s over a period of 3s in the participant's walking direction, following an ogive function (μ =0, σ =0.5 s) fit to previous data. On perturbation trials, after 2s a subset (S) of the 12 neighbors then changed their heading direction (\pm 10° left or right) or speed (\pm 0.3 m/s) over a period of 0.5s, following another ogive function (μ =0, σ =0.083 s).

Procedure

Participants were instructed to walk as naturally as possible, to treat the virtual pedestrians as if they were real people, and to stay together with the crowd. On each trial, the participant walked to the start pole and faced the orienting pole. After 2s, the poles disappeared and the virtual crowd appeared; 1s later, a verbal command ("Begin") was played and the virtual crowd began walking. The display continued until the participant had walked about 12m; a verbal command ("End") signaled the end of the trial. In each experiment, there were 8 heading trials and 8 speed trials per condition, presented in a randomized order, with 80 trials in each 1-hour session.

Data Processing

197

198

199

200

201

202

203

204

205

206

207

208

209

210

211

212

213

214

215

216

217

218

For each trial, the time series of head position in the horizontal X-Y plane were filtered using a forward and backward 4th-order low-pass Butterworth filter to reduce occasional tracker error and oscillations due to the step cycle. Time series of walking speed, heading direction, and their rates of change, were then computed from the filtered position data. A 1.0 Hz cutoff was used for computing speed to reduce anterior-posterior oscillations on each step (Rio et al., 2014), while a 0.6 Hz cutoff was used for computing heading to reduce lateral oscillations on each stride (Fajen & Warren, 2003). To eliminate 'endpoint error', the time series were extended by 2s using linear extrapolation based on the last 0.5s of data for filtering only (Vint & Hinrichs, 1996). Dependent measures were the participant's change in heading or walking speed in response to a perturbation. Change in heading was measured by computing the lateral deviation, subtracting the participant's final lateral position on a perturbation trial (1s before the end of the trial) from their mean final lateral position on all control trials. Right and left turn trials were then collapsed by multiplying the lateral deviation on left turns by -1. Change in speed was computed by subtracting the participant's mean final speed on a perturbation trial (1.5 to 0.5s before the end of the trial) from their mean final speed on all control trials in the corresponding distance condition. Slow and fast trials were collapsed by multiplying the final speed on slow trials by -1. However, we noted a small asymmetry, with a greater speed change in response to neighbors decelerating (for Exp. 2, S=12, M=0.31 m/s, SD=0.09) than accelerating (M=0.20 m/s, SD=0.13; t(19)=3.11, p<.01) from the same initial distance; Rio et al. (2014) attributed this to Euclid's law of perspective, which produces a higher rate of optical expansion than contraction. The collapsed data were analyzed using 1-Way Repeated Measures ANOVA in Exp. 1 (main

effect of number of perturbed neighbors) and 2-Way RM ANOVA in Exp. 2 (main effects of

Rio, Dachner, & Warren

number and distance of perturbed neighbors) and Exp. 3 (main effects of eccentricity and distance of perturbed neighbors), with generalized eta squared (η_G^2) as a measure of effect size, in R statistical software.

Experiment 1: Number of Perturbed Neighbors

Experiment 1 tested the superposition hypothesis by manipulating the number of neighbors in the perturbed subset (S=0,3,6,9,12), randomly varying their positions on each trial. Superposition predicts that, as the number (or proportion) of perturbed neighbors increases, the participant's response should increase linearly. There were thus 5 subset conditions and a total of 80 trials.

Results

There was a significant effect of the number of perturbed neighbors on the participants' lateral deviation, $(F(4,36) = 95.33, p < .001, \eta_G^2 = 0.86)$, consistent with a linear combination of neighbor influences (Figure 2a). Similarly, there was a significant effect of number of perturbed neighbors on the participants' change in speed $(F(4,36) = 22.17, p < .001, \eta_G^2 = 0.66)$ (see Figure S1 in Supplementary Material). Indeed, in both cases the mean response increased linearly with the size of the perturbed subset (r=0.99) for both heading and speed).

The results of Experiment 1 demonstrate that velocity alignment is consistent with the superposition hypothesis. That is, the participant's heading and speed response is a linear combination of responses to each neighbor. Given that the total number of neighbors was constant (N=12), the response could depend on either the absolute number or the proportion of neighbors perturbed; subsequent research (in preparation) suggests the latter.

244

Experiment 2: Distance of Perturbed Neighbors

245

246

247

248

249

250

Experiment 2 tested the distance hypothesis by perturbing neighbors in the near zone and/or the far zone (Figure 1c). The distance hypothesis predicts that perturbing neighbors in the near zone should elicit a greater response from the participant than perturbing those in the far zone. The design of Experiment 2 was thus 2 distances (\sim 1.5m, \sim 3.5m) x 5 subsets (S=0,3,6,9,12), yielding 10 conditions and a total of 160 trials.

251

252

253

254

255

256

257

258

259

260

261

262

263

264

265

266

Results

We found a significant effect of the distance of perturbed neighbors on the participants' lateral deviation $(F(1.9) = 71.57, p < .001, \eta_0^2 = 0.49)$, consistent with the hypothesis that neighbor influence decreases with distance (Figure 2b). Once again, there was a significant effect of subset size on lateral deviation (F(4.36) = 244.66, p < .001, $\eta_G^2 = 0.89$), consistent with superposition.

Because there were only 5 neighbors in the near zone and 7 in the far zone, larger subsets actually perturbed neighbors in both zones. Thus, for a stronger test of the distance hypothesis, we performed a sub-analysis of the smaller subsets alone (S=0,3,6, left side of Figure 2b). The results confirmed a significantly greater response to perturbed neighbors in the near zone than the far zone (F(1,9)=69.99, p<.001, $\eta_G^2=0.68$), as well as a significant effect of subset size $(F(2.18)=90.93, p<.001, \eta_G^2=0.70)$, and a significant interaction (F(2.18)=45.58, p<.001, q) $\eta_G^2 = 0.58$).

Similarly, we found a significant effect of neighbor distance on the participants' change in speed $(F(1,9) = 22.93, p < .001, \eta_G^2 = 0.25)$, as well as a significant effect of subset size (F(4,36)

Rio, Dachner, & Warren

= 34.28, p < .001, η_G^2 =0.72) (Figure 2c). A sub-analysis of the smaller subsets (S=0,3,6) confirmed a significantly greater response to neighbors in the near zone than the far zone (F(1,9)=60.15, p<.001, η_G^2 =0.54), a significant effect of subset size (F(2,18)=50.67, p<.001, η_G^2 =0.64), and a significant interaction (F(2,18)=2.70, p<.001, η_G^2 =0.33).

The results of Experiment 2 demonstrate that coupling strength decreases with neighbor distance for both heading and speed, consistent with the distance hypothesis. Visually, this decrease might be attributed to lower angular velocities due to the laws of perspective, to greater occlusion of far neighbors, or both – a question we are currently pursuing. In sum, the local neighborhood can be characterized by the superposition of binary interactions, with a coupling strength that decreases with distance.

Experiment 3: Eccentricity of Perturbed Neighbors

In Experiment 3, we tested the eccentricity hypothesis by selectively perturbing neighbors in 30° horizontal sectors of the display. There were five overlapping sectors (centered on -30° , -15° , 0° , $+15^{\circ}$, and $+30^{\circ}$, left to right). The eccentricity hypothesis predicts that neighbors in the central sector (0°) should elicit the greatest response, while responses to neighbors in more peripheral sectors ($\pm 15 \text{K}$, $\pm 30^{\circ}$) should progressively decrease. We also repeated the distance manipulation by perturbing neighbors in the near zone (M = 1.23 neighbors, SD = 0.73) or the far zone (M = 2.18 neighbors, SD = 0.81) of a given sector. The design was thus 5 eccentricity x 2 distance conditions, plus a no-perturbation control, yielding 11 conditions and a total of 176 trials.

Results

290

There was no overall effect of eccentricity on the participants' mean lateral deviation 291 $(F(4,36) = 1.94, p > .05, \eta_0^2 = 0.04$; Figure 3a). We again observed a significant effect of 292 neighbor distance $(F(1.9) = 20.19, p < .01, \eta_G^2 = 0.14)$, but there was also a significant interaction 293 $(F(4,36) = 3.65, p < .05, \eta_G^2 = 0.14)$. A simple effects analysis revealed a significant eccentricity 294 effect in the Far condition (F(4,36)=3.63, p<.05, $\eta_G^2=0.25$), but not in the Near condition 295 $(F(4,36)=1.22, p>.05, \eta_G^2=0.08)$. Moreover, the distance effect was only significant at 296 eccentricities of -30° and +30° (p < .01). 297 Similarly, we found no overall effect of eccentricity on the participants' change in speed 298 $(F(4,36) = 0.86, p > .05, \eta_G^2 = 0.04$; Figure 3b). There was again a significant effect of distance 299 $(F(1.9) = 14.15, p < .01, \eta_0^2 = 0.10)$, but no interaction $(F(4.36) = 0.95, p > .05, \eta_0^2 = 0.00)$; 300 responses were greater to near neighbors than far neighbors at all eccentricities. Simple effects 301 tests did not reveal an eccentricity effect in either the near or the far zone (both p > .05, $\eta_G^2 = 0.04$). 302 The results do not provide convincing evidence for the eccentricity hypothesis. The only 303 consistent effect occurs with heading perturbations of far neighbors at larger eccentricities (red 304 curve in Figure 3a). We suggest this effect may be due to the laws of perspective, similar to one 305 we observed in binary following (Dachner & Warren, 2017). If a neighbor straight ahead (0° 306 eccentricity) turns 10° left or right, they drift laterally in the field of view with a given angular 307 velocity; a neighbor at a 30° eccentricity would have a smaller mean angular velocity, which 308 would decrease even further with distance. The reduced response in the Far condition may thus 309 be atributable to reduced optical motion. In contrast, speed perturbations produce optical 310 expansion/contraction that appears to be similar over this range of eccentricities, although it too 311

Rio, Dachner, & Warren

decreases with distance (Figure 3b). These visual effects might explain the pattern of results in Experiment 3.

Taken together, the experimental findings are consistent with the superposition of multiple neighbors, with a coupling strength that decreases with distance but not eccentricity.

Observational Data on a Human 'Swarm'

To compare these experimental results with observations of crowd behavior, we collected motion capture data on collective motion in a human 'swarm' scenario. We recorded three groups of participants walking together for periods of 2 min. To investigate the distance and eccentricity hypotheses, we computed pairwise statistics between a central participant and each neighbor as a function of their relative spatial positions.

325 Methods

Participants

One group of 16 participants (6F, 10M) and two groups of 20 participants (10F, 10M) were tested in separate sessions as part of a larger study.

Apparatus

The groups were tested in a large hall with a 14 x 20 m tracking area marked on the floor with red tape. Each participant wore a bicycle helmet with a unique constellation of 5 reflective markers on 30-40 cm stalks. Head position was recorded at 60 Hz with a 16-camera infrared motion capture system (Qualisys Oqus).

Procedure

335

336

337

338

339

340

341

342

343

344

345

346

347

348

349

350

351

352

Participants were instructed to walk about the tracking area at a normal speed, veering randomly left and right, while staying together as a group. They began each trial in random positions in a 7x7m start box marked on the floor (~2m interpersonal distance (IPD)) or a 4x4m start box (~1m IPD). At a verbal "go" signal, they started walking for 2 min, until a "stop" signal.

Data processing

We analyzed three 2m IPD trials in detail, a total of 6 min of data. 3D head positions were successfully recovered on 88% of frames, and the time series for each participant were processed as before. Walking speed did not vary appreciably, and was not analyzed further. To measure local coordination, we computed the absolute value of the difference in heading direction between the 'central participant' nearest the center of the swarm and each neighbor on each frame, thereby minimizing edge effects (Cavagna et al., 2010). To estimate response times, windowed cross-correlations (1s traveling window) and optimal delays between the central participant and each neighbor were also computed. These measurements were averaged across all frames and plotted in heat maps with the central participant at the origin (0,0) heading upward; each cell thus represents the mean statistic for all participants occupying that relative spatial location in 6 min of data.

353

354 Results

355

356

357

A heat map of mean absolute heading difference appears in Figure 4a. It is immediately apparent that the neighborhood is circularly symmetric, not elliptical. The mean heading

Rio, Dachner, & Warren

difference is quite small, 15-25°, within a 2m radius, but increases to 30-40° at a radius of 3-4m. There is thus close coordination with near neighbors that decreases with distance.

To estimate the decay in coupling strength with distance, we computed the mean heading difference at each radius in the heat map, scaled it (range 0 to 1) and subtracted it from 1, and plotted the result as a function of radial distance (Figure 4c). The coupling strength w_i to each neighbor decays exponentially with distance, closely fit by the equation

$$w_i = \frac{a}{e^{\omega d_i} + a} \tag{3}$$

where d_i is the distance of neighbor i, $\omega=1.3$ is the decay rate, and a=9.2 is a constant ($r^2=0.98$).

Given that the human field of view is about 180°, however, a pedestrian is visually coupled only to neighbors in front of them. This uni-directional coupling is apparent from the heat map of mean time delay for the same 6 min of data (Figure 4b). Time delays in the upper half of the map are positive, indicating that the central participant turned after the neighbors ahead, whereas those in the lower half are negative, indicating that neighbors behind turned after the central participant. Mean time delays are about 1s within a 1.5-2m radius, increasing to 1-3s at 3-4m. For binary following, Dachner & Warren (2014) reported mean delays of 0.98s to a neighbor who turns 2m ahead, and 1.33s to a neighbor 4m ahead. This suggests that the central participant's response to some (possibly occluded) far neighbors may be mediated by an intervening neighbor, yielding a chain of response times.

Modelling Interactions in a Local Neighborhood

The present findings enable us to formulate a model of the local neighborhood (Figure 5a). Specifically, given superposition, we propose that a pedestrian's linear (or angular) acceleration

is a weighted average of the difference between their current speed (heading) and that of each neighbor. By substituting the alignment dynamics (Equations 1-2) into this neighborhood model,

we can derive the local interactions that generate collective motion,

$$\ddot{r}_p = \frac{c}{n} \sum_{i=1}^n w_i (\dot{r}_i - \dot{r}_p) \tag{4}$$

$$\ddot{\phi}_p = -\frac{k}{n} \sum_{i=1}^n w_i sin(\phi_i - \phi_p)$$
 (5)

where *n* denotes the number of neighbors in the pedestrian's neighborhood (within a 5m radius, $\pm 90^{\circ}$ from current heading). The weight w_i has a value of 1 at 0m and decays exponentially with the neighbor's radial distance, in accordance with Equation 3. To estimate the gain parameters c, k at a theoretical distance of 0m, we fit our previous data on binary following separately for distances of 1, 2, and 4m, and linearly extrapolated to 0m, obtaining c=3.61 and k=3.15.

To test this 'soft radius' model, we first determined how closely it reproduces the data from Experiments 1 and 2, and then how well it predicts individual trajectories in the more variable human swarm, with fixed parameters.

391

392

380

381

382

383

384

385

386

387

388

389

390

Simulation Methods

393

394

395

396

397

398

399

Each trial from Experiments 1 and 2 was simulated by taking the virtual neighbors' distance and speed (heading) as input at each time step, and computing a time series of the model's speed (heading) in accordance with Equation 4 (Equation 5). To reduce the effects of gait oscillations and tracker error on individual trials, a mean time series was computed for each participant in each condition and compared with the mean model time series in the corresponding condition, using the correlation coefficient (Pearson's r) and the root of the mean squared error (RMSE).

Rio, Dachner, & Warren

The same model was used to simulate individual trajectories in the human swarm data. First, we identified 10s segments in which a participant had ≥7 neighbors in their neighborhood who were continuously tracked at speeds ≥0.2 m/s; this yielded 14 segments of 2m IPD data and 17 segments of 1m IPD data. At the start of each segment, the model was initialized with the participant's position, speed, and heading. The distance, speed, and heading of every neighbor was treated as input, and the model computed the participant's speed, heading, and change in position on each time step. We computed the correlation and RMSE between the individual model and human time series, and the mean position error (distance between model and human), over the 10s segment.

410 Results

The correlations between the model and human in Experiment 1 were strong, with means of r=0.88 (RMSE=0.05 m/s) for speed and r=0.81 (RMSE=1.94°) for heading in the perturbation conditions. In Experiment 2, the mean correlations were even higher, with r=0.90 (RMSE=0.06 m/s) for speed and r=0.88 (RMSE=2.06°) for heading. The model thus closely reproduces the temporal evolution of a pedestrian's response to their neighbors (Figure S2, S3). Moreover, model predictions of the final stabilized heading and speed (mean of last 2s in time series) were virtually identical to the mean human data, as shown in Figures 5b and 5c for Experiment 2. The predicted value is contained within the 95% confidence interval for the human data, indicating that the data do not differ significantly from the model.

The model also predicts individual trajectories in the human swarm. A sample trajectory from a 10s segment of swarm data appears in Figure 6 (also Figure S4). For the 2m IPD, the

mean correlations between model and human time series were r=0.90 (RMSE=31.16°) for heading, and r=0.65 (RMSE=0.19 m/s) for speed³. Position error accumulated from a mean of 0.27m during the first 3s to a mean of 0.93m for the 10s segments. The model also generalized to the 1m IPD, with mean correlations of r=0.93 (RMSE=27.56°) for heading and r=0.60 (RMSE=0.16 m/s) for speed; mean position error increased from 0.21m during the first 3s to 0.70m over 10s.

In sum, the neighborhood model accounts for the coordination of heading and speed between individuals in a crowd, and consequently the emergence of collective motion.

Discussion

The experimental results demonstrate that a pedestrian's interactions with multiple neighbors are linearly combined, in accordance with superposition. At the same time, neighbor influence decreases with distance, going to zero by 5m. On the other hand, influence does not appear to depend on eccentricity within the field of view. In contrast to prey species with nearly panoramic vision, yielding bi-directionally coupled flocks and schools, humans typically have a 180° field of view and are uni-directionally coupled to neighbors ahead. This has implications for the causal network in human crowds.

These findings led us to model the local neighborhood as a weighted average of neighbors (Equations 4, 5), in which the weights decrease exponentially with radial distance (Equation 3). Together with our previous results on alignment dynamics (Equations 1 and 2), this enabled us to

³ These values reflect comparisons between individual time series, rather than mean time series, yielding larger RMSEs due to gait oscillations and tracker error. Speed correlations are lower because there was little variation in speed in the swarm.

Rio, Dachner, & Warren

simulate the local interactions underlying collective crowd motion. The model not only reproduces participant responses in a virtual crowd, but generalizes to individual trajectories in a human swarm. Despite the fact that swarm motion was more variable and some neighbor data were missing, leading to an accumulation of position error, the heading correlation was highly robust.

The model neighborhood decays exponentially with radial distance, creating a 'soft' radius. This neighborhood structure contrasts with previous theoretical models that presume an alignment zone with a constant coupling strength and a hard radius. Our empirical model agrees with the theoretical equation of Cucker and Smale (2007), who showed that a weighted-average model with a sufficiently gradual decay converges to collective motion.

A number of further questions remain. First, the present data do not resolve the issue of whether the neighborhood is defined by metric distance (e.g. meters), or topological distance (number of neighbors) as suggested by some analyses of bird flocks (Ballerini et al., 2008; but see Evangelista, Ray, Raja, & Hedrick, 2017). Second, although an 'attraction' rule appears to play a role in flocking (Hildenbrandt et al., 2010; Lukeman et al., 2010), an analogue for moving crowds has not yet been investigated. Finally, at present, physical distance is a proxy for visual information that depends on perspective or occlusion; we are currently incorporating optical variables into the model. We plan to address these questions in future reports.

463 Conclusions

We conclude that the local neighborhood of interaction in human crowds is circularly symmetric, with a uni-directional coupling to multiple neighbors within $\pm 90^{\circ}$ of the current

Rio.	Dachner,	&	Warren

heading. Their influences are superposed as a weighted average, where the weight decays exponentially with distance. Combining this 'soft' neighborhood with the alignment dynamics yields the first experiment-driven, bottom-up model of collective motion in human crowds. This behavioral dynamics model accounts for individual trajectories in virtual and real crowds, and generates collective motion, consistent with principles of self-organization. It is thus possible to experimentally decipher the local interactions that underlie collective crowd behavior.

Ethics

The research protocol was approved by Brown University's Institutional Review Board, in accordance with the principles expressed in the Declaration of Helsinki. Informed consent was obtained from all participants, who were paid for their participation.

Data accessibility

The data supporting this article may be accessed from the Brown University Digital Repository [https://repository.library.brown.edu/studio/item/bdr:735090/].

Competing interests

486 No competing interests.

Authors' contributions

490

491

492

493

Rio, Dachner, & Warren

23

KR contributed to the conception and design of the experiments, created the visual displays, collected the data, performed the data analysis, and co-wrote the manuscript. GD performed the model simulations and contributed to the data analysis. WW contributed to the conception and design of the experiments and the data analysis, and co-wrote the manuscript. All authors gave final approval for publication.

494

495

496

497

Acknowledgements

Thanks to Arturo Cardenas, Stéphane Bonneaud, Adam Kiefer, Michael Fitzgerald, and all those who helped collect and process Sayles Swarm data.

498

499

Funding

The research was supported by National Institutes of Health (USA) grant R01EY010923 and National Science Foundation (USA) grant BCS-1431406 to WW, and a Link Foundation fellowship to KR.

Refe	ren	ces
------	-----	-----

503

504 505	Ballerini, M., Cabibbo, N., Candelier, R., Cavagna, A., Cisbani, E., Giardina, I., Zdravkovic
506	V. (2008). Interaction ruling animal collective behavior depends on topological rather
507	than metric distance: Evidence from a field study. Proceedings of the National Academy
508	of Sciences, 105(4), 1232-1237.
509	Bonneaud, S., & Warren, W. H. (2014). An empirically-grounded emergent approach to
510	modeling pedestrian behavior. In U. Weidmann, U. Kirsch, & M. Schreckenberg (Eds.),
511	Pedestrian and Evacuation Dynamics 2012 (pp. 625-637): Springer International.
512	Cavagna, A., Cimarelli, A., Giardina, I., Parisi, G., Santagati, R., & Stefanini, F. (2010). Scale-
513	free correlations in starling flocks. Proceedings of the National Academy of Sciences,
514	<i>107</i> (26), 11865-11870.
515	Couzin, I. D., & Krause, J. (2003). Self-organization and collective behavior in vertebrates.
516	Advances in the Study of Behavior, 32, 1-75.
517	Couzin, I. D., Krause, J., James, R., Ruxton, G. D., & Franks, N. R. (2002). Collective memory
518	and spatial sorting in animal groups. Journal of Theoretical Biology, 218, 1-11.
519	Cucker, F., & Smale, S. (2007). Emergent behavior in flocks. IEEE Transactions on Automatic
520	Control, 52(5), 852-862.
521	Czirók, A., & Vicsek, T. (2000). Collective behavior of interacting self-propelled particles.
522	Physica A, 281, 17-29.
523	Dachner, G., & Warren, W. H. (2014). Behavioral dynamics of heading alignment in pedestrian
524	following. Transportation Research Procedia, 2, 69-76.
525	Dachner, G., & Warren, W. H. (2017). A vision-based model for the joint control of speed and
526	heading in pedestrian following. Journal of Vision, 17(10), 716.

Evangelista, D. J., Ray, D. D., Raja, S. K., & Hedrick, T. L. (2017). Three-dimensional 527 528 trajectories and network analyses of group behaviour within chimney swift flocks during approaches to the roost. *Proc. R. Soc. B*, 284(1849), 20162602. 529 530 Fajen, B. R., & Warren, W. H. (2003). Behavioral dynamics of steering, obstacle avoidance, and route selection. Journal of Experimental Psychology: Human Perception and 531 Performance, 29, 343-362. 532 Fajen, B. R., & Warren, W. H. (2007). Behavioral dynamics of intercepting a moving target. 533 Experimental Brain Research, 180, 303-319. 534 Gautrais, J., Ginelli, F., Fournier, R., Blanco, S., Soria, M., Chaté, H., & Theraulaz, G. (2012). 535 Deciphering interactions in moving animal groups. PLoS Comput Biology, 8(9), 536 e1002678. 537 538 Gérin-Lajoie, M., Richards, C. L., & McFadyen, B. J. (2005). The negotiation of stationary and moving obstructions during walking: Anticipatory locomotor adaptations and 539 preservation of personal space. *Motor Control*, 9, 242-269. 540 541 Haken, H. (1983). Synergetics, an introduction: Nonequilibrium phase transitions and selforganization in physics, chemistry, and biology (3rd ed.). New York: Springer-Verlag. 542 Helbing, D., Buzna, L., Johansson, A., & Werner, T. (2005). Self-organized pedestrian crowd 543 dynamics: Experiments, simulations, and design solutions. Transportation science, 39(1), 544 1-24. 545 Helbing, D., & Molnár, P. (1995). Social force model of pedestrian dynamics. *Physical Review* 546 *E*, *51*, 4282-4286. 547 Hildenbrandt, H., Carere, C., & Hemelrijk, C. K. (2010). Self-organized aerial displays of 548 549 thousands of starlings: A model. *Behavioral Ecology*, 21(6), 1349-1359.

550 Hsieh, Y.-H., Ngai, K. M., Burkle, F. M., & Hsu, E. B. (2009). Epidemiological characteristics 551 of human stampedes. Disaster medicine and public health preparedness, 3(04), 217-223. Lemercier, S., Jelic, A., Kulpa, R., Hua, J., Fehrenbach, J., Degond, P., ... Pettré, J. (2012). 552 Realistic following behaviors for crowd simulation. Computer Graphics Forum, 553 31(2pt2), 489-498. 554 Lukeman, R., Li, Y.-X., & Edelstein-Keshet, L. (2010). Inferring individual rules from collective 555 behavior. Proceedings of the National Academy of Sciences, 107(28), 12576-12580. 556 Moussaïd, M., Guillot, E. G., Moreau, M., Fehrenbach, J., Chabiron, O., Lemercier, S., . . . 557 Theraulaz, G. (2012). Traffic instabilities in self-organized pedestrian crowds. *PLoS* 558 Comput Biology, 8(3), e1002442. 559 Moussaïd, M., Helbing, D., & Theraulaz, G. (2011). How simple rules determine pedestrian 560 561 behavior and crowd disasters. Proceedings of the National Academy of Sciences, 108(17), 6884-6888. 562 Ondrej, J., Pettré, J., Olivier, A.-H., & Donikian, S. (2010). A synthetic-vision based steering 563 564 approach for crowd simulation. ACM Transactions on Graphics, 29(4), 123: 121-129. Pelechano, N., Allbeck, J. M., & Badler, N. I. (2007). Controlling individual agents in high-565 density crowd simulation. Proceedings of the 2007 ACM SIGGRAPH/Eurographics 566 Symposium on Computer Animation, 99-108. 567 Reynolds, C. W. (1987). Flocks, herds, and schools: a distributed behavioral model. *Computer* 568 569 Graphics, 21, 25-34. Rio, K., Rhea, C., & Warren, W. H. (2014). Follow the leader: Visual control of speed in 570 pedestrian following. Journal of Vision, 14(2), 4:1-16. 571

Rio	Dachner.	&	Warren
IXIO.	Dacinici.	œ	vv an cn

PLoS One, 7(6), e38588.

591

592

27

Schellinck, J., & White, T. (2011). A review of attraction and repulsion models of aggregation: 572 Methods, findings and a discussion of model validation. Ecological Modeling, 222, 1897-573 1911. 574 Sumpter, D. J. T. (2006). The principles of collective animal behavior. *Philosophical* 575 Transactions of the Royal Society B, 361, 5-22. 576 Sumpter, D. J. T., Mann, R. P., & Perna, A. (2012). The modelling cycle for collective animal 577 behaviour. Interface Focus, 2(6), 764-773. 578 Vicsek, T., Czirók, A., Ben-Jacob, E., Cohen, I., & Shochet, O. (1995). Novel type of phase 579 transition in a system of self-driven particles. *Physics Review Letters*, 75(6), 1226-1229. 580 Vicsek, T., & Zafeiris, A. (2012). Collective motion. *Physics Reports*, 517, 71-140. 581 Vint, P. F., & Hinrichs, R. N. (1996). Endpoint error in smoothing and differentiating raw 582 583 kinematic data: an evaluation of four popular methods. J Biomech, 29(12), 1637-1642. Warren, W. H. (2006). The dynamics of perception and action. Psychological Review, 113, 358-584 389. 585 Warren, W. H., & Fajen, B. R. (2008). Behavioral dynamics of visually-guided locomotion. In 586 A. Fuchs & V. Jirsa (Eds.), Coordination: Neural, behavioral, and social dynamics. 587 Heidelberg: Springer. 588 Weitz, S., Blanco, S., Fournier, R., Gautrais, J., Jost, C., & Theraulaz, G. (2012). Modeling 589 collective animal behavior with a cognitive perspective: A methodological framework. 590

Figure Captions

593

594	Figure 1. (a) Virtual crowd display from participant's view, and (b) an aerial view. (c) Diagram
595	of a heading perturbation with S=3.
596	
597	Figure 2. (a) Experiment 1: Heading perturbations. Mean absolute lateral deviation as a function
598	of the number of neighbors in the perturbed subset S. (b) Experiment 2: Heading perturbations.
599	Mean absolute lateral deviation as a function of the number and distance of perturbed neighbors.
600	(c) Experiment 2: Speed perturbations. Mean absolute change in speed as a function of same.
601	Error bars=SE of mean.
602	
603	Figure 3. Results of Experiment 3: (a) Heading perturbations. Mean absolute lateral deviation as
604	a function of the eccentricity and distance of perturbed neighbors. (b) Speed perturbations. Mean
605	absolute change in speed as a function of same. Error bars=SE of mean.
606	
607	Figure 4. Mean results for 6 min of human 'swarm' data. (a) Heat map of absolute heading
608	difference between each neighbor and central participant (cell=0.5x0.5m). (b) Heat map of time
609	delay, neighbor-central participant (cell=0.33x0.33m). (c) Coupling strength (scaled heading
610	difference) as a function of radial distance, from data in a ; curve is exponential fit ($r^2 = 0.98$).
611	
612	Figure 5. (a) Diagram of neighborhood model. Simulation Experiment 2: (b) Heading
613	perturbations. Mean absolute final heading as a function of number and distance of perturbed
614	neighbors. (c) Speed perturbations. Mean absolute final speed as a function of same. Shaded
615	regions = 95% CI for human data.

Rio	Dachner,	&	Warren
TUO.	Dacinici.	œ	vv arren

616

Figure 6. Simulation of sample segment from the human 'swarm' (IPD=1m). (a) Path in space,
mean position error=0.13m (dots at 1s intervals). (b) Time series of speed, r =0.95, RMSE=0.10
m/s. (c) Time series of heading, r =0.99, RMSE=11.84°. Participant = solid red curve, model =
dashed blue curve, neighbors = black curves; O=starting positions, X=final positions.

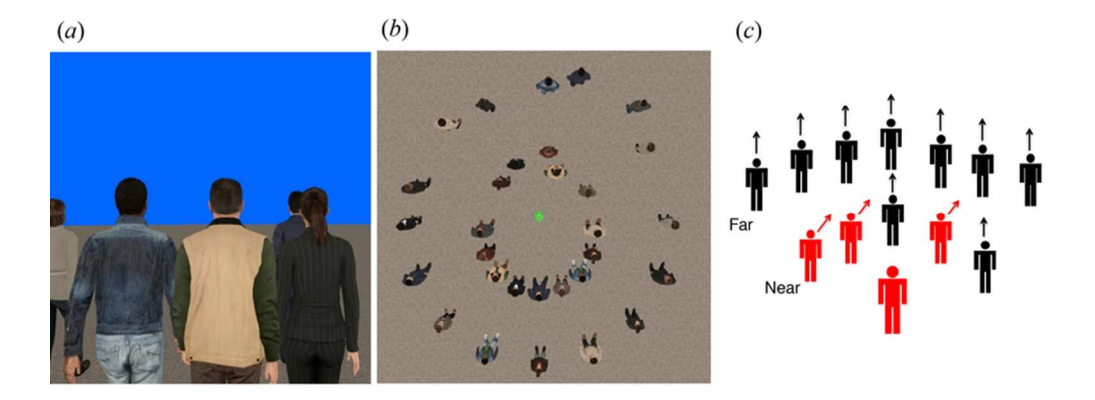


Figure 1. (a) Virtual crowd display from participant's view, and (b) an aerial view. (c) Diagram of a heading perturbation with S=3.

75x32mm (300 x 300 DPI)

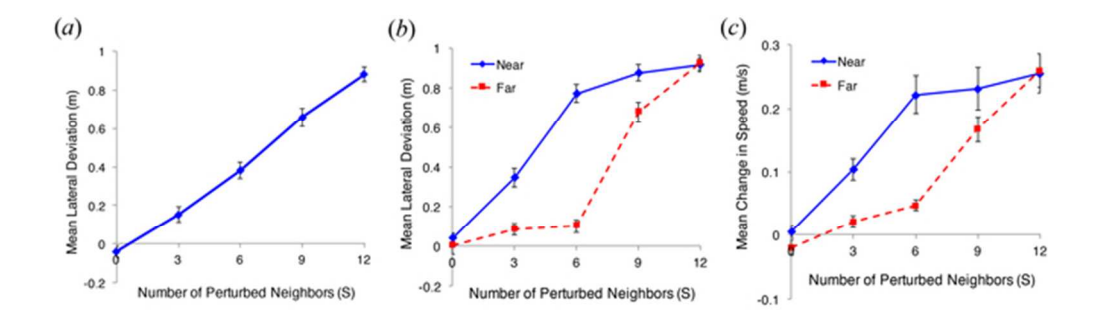


Figure 2. (a) Experiment 1: Heading perturbations. Mean absolute lateral deviation as a function of the number of neighbors in the perturbed subset S. (b) Experiment 2: Heading perturbations. Mean absolute lateral deviation as a function of the number and distance of perturbed neighbors. (c) Experiment 2: Speed perturbations. Mean absolute change in speed as a function of same. Error bars=SE of mean.

55x17mm (300 x 300 DPI)

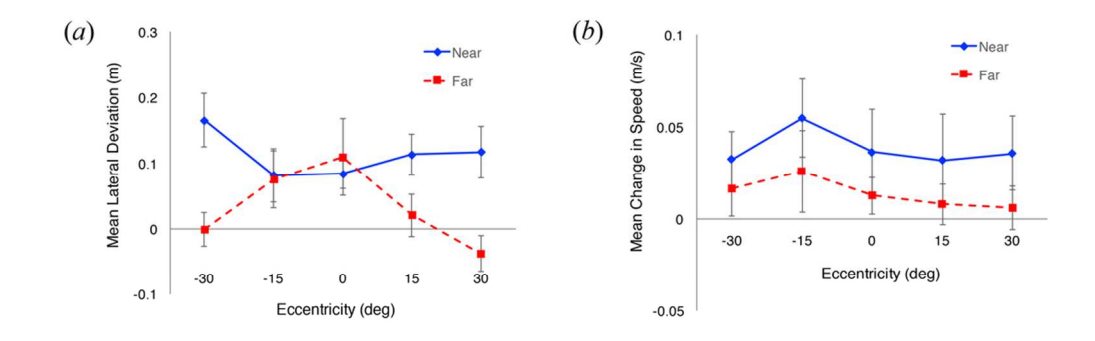


Figure 3. Results of Experiment 3: (a) Heading perturbations. Mean absolute lateral deviation as a function of the eccentricity and distance of perturbed neighbors. (b) Speed perturbations. Mean absolute change in speed as a function of same. Error bars=SE of mean.

95x57mm (300 x 300 DPI)

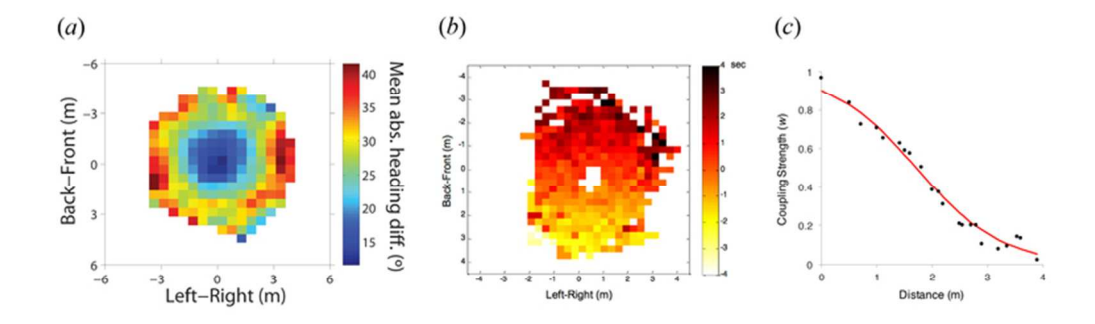


Figure 4. Mean results for 6 min of human 'swarm' data. (a) Heat map of absolute heading difference between each neighbor and central participant (cell=0.5x0.5m). (b) Heat map of time delay, neighbor-central participant (cell=0.33x0.33m). (c) Coupling strength (scaled heading difference) as a function of radial distance, from data in a; curve is exponential fit ($r^2 = 0.98$).

64x23mm (300 x 300 DPI)

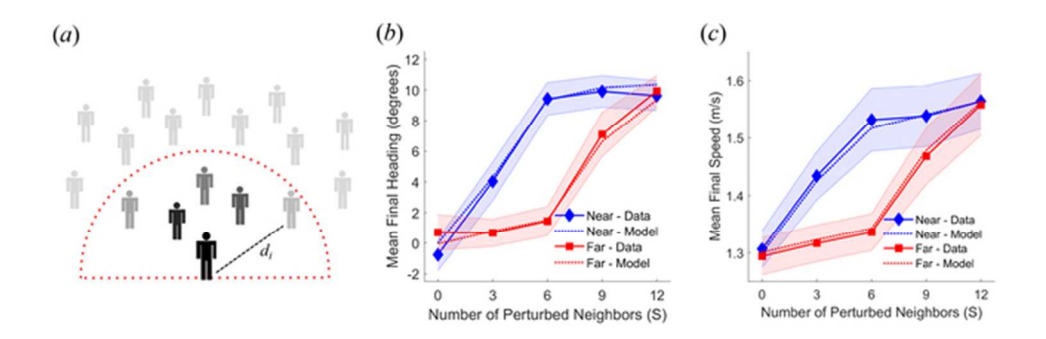


Figure 5. (a) Diagram of neighborhood model. Simulation Experiment 2: (b) Heading perturbations. Mean absolute final heading as a function of number and distance of perturbed neighbors. (c) Speed perturbations. Mean absolute final speed as a function of same. Shaded regions = 95% CI for human data.

57x18mm (300 x 300 DPI)

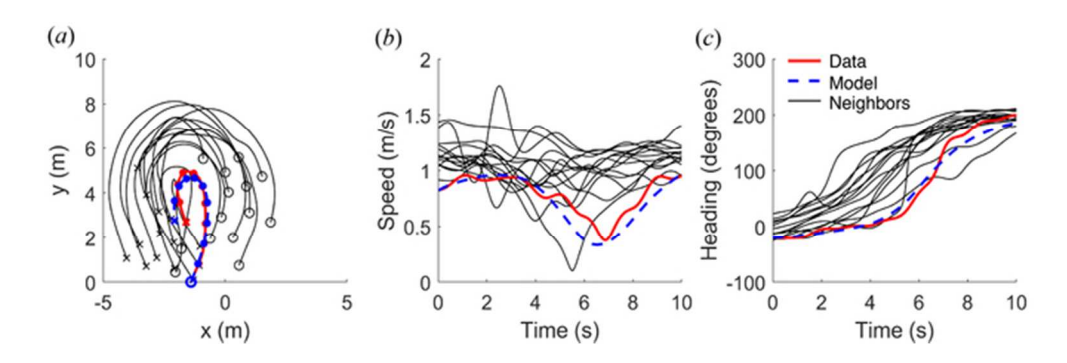


Figure 6. Simulation of sample segment from the human 'swarm' (IPD=1m). (a) Path in space, mean position error=0.13m (dots at 1s intervals). (b) Time series of speed, r=0.95, RMSE=0.10 m/s. (c) Time series of heading, r=0.99, RMSE=11.84°. Participant = solid red curve, model = dashed blue curve, neighbors = black curves; O=starting positions, X=final positions.

57x18mm (300 x 300 DPI)

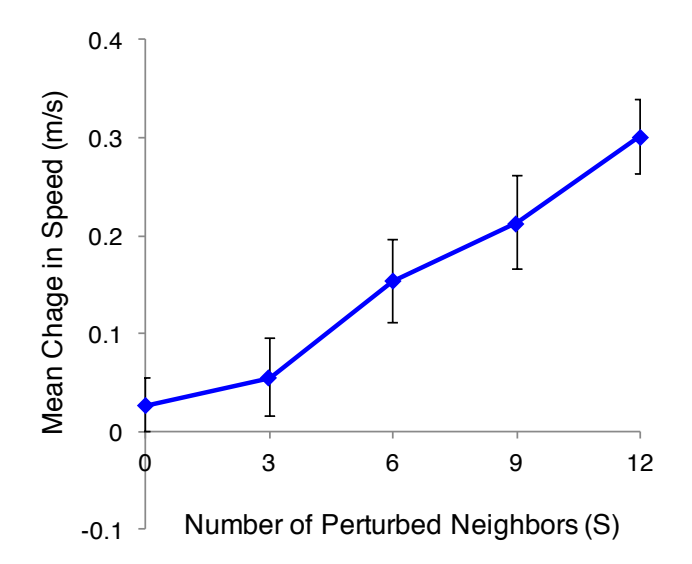


Figure S1. Speed perturbations in Experiment 1: Mean absolute change in speed as a function of the number of neighbors in the perturbed subset S. This figure is paired with Figure 2a in Rio, Dachner, & Warren. Error bars=SE of mean.

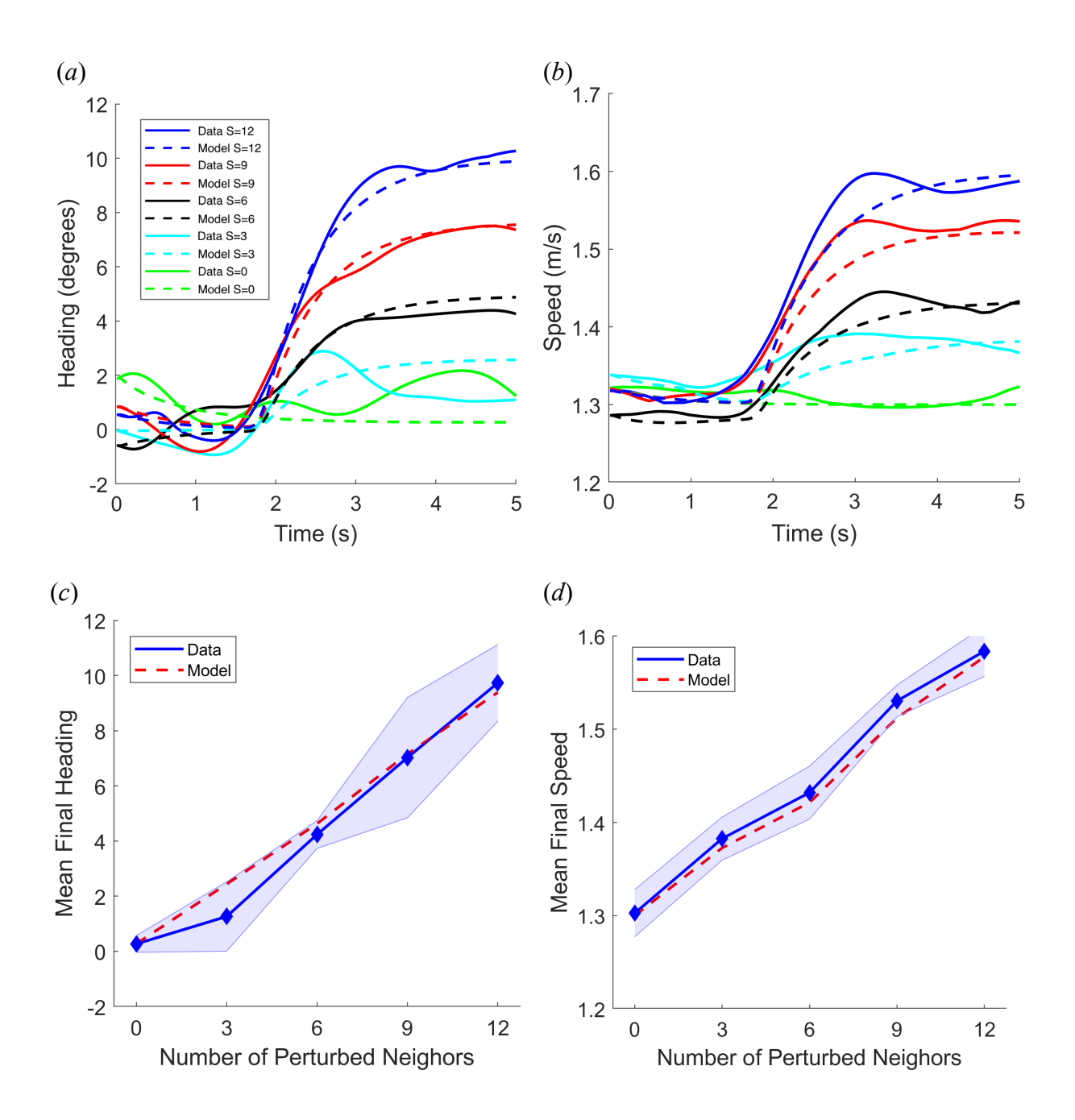


Figure S2. Simulations of heading perturbations and speed perturbations in Experiment 1. *Top:* Mean time series of (a) heading and (b) speed for human data (solid curves) and model (dashed curves) at each subset size S (number of perturbed neighbors, colored curves). *Bottom:* Mean absolute final (c) heading and (d) speed as a function of the number of perturbed neighbors S. Shaded regions = 95% CI for human data.

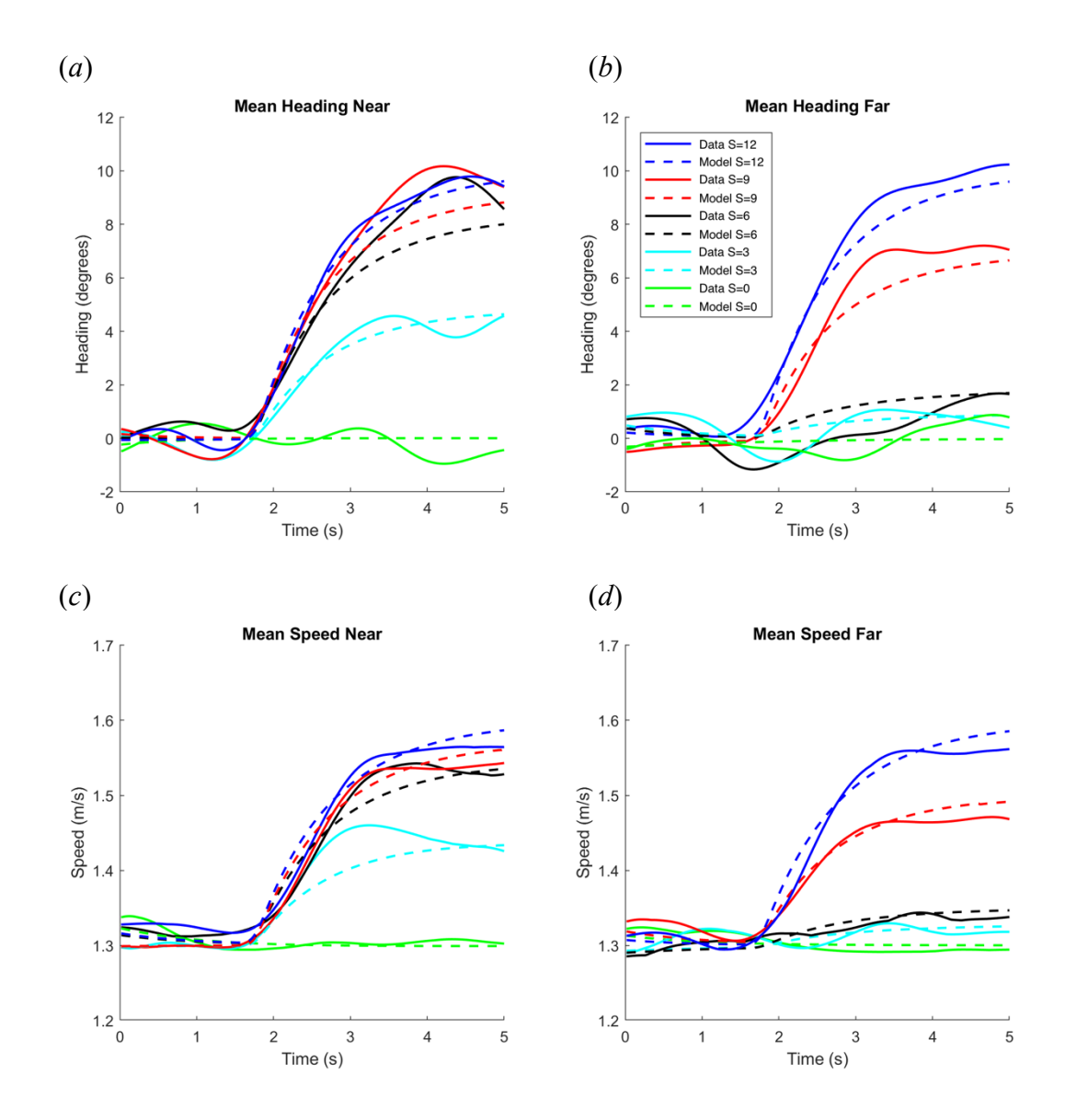


Figure S3. Mean time series for human data (solid curves) and model (dashed curves) in Experiment 2. *Top*: Mean time series of heading for each subset size S (number of perturbed neighbors, colored curves) in (a) the Near condition (~1.5m) and (b) the Far condition (~3.5m). *Bottom:* Mean time series of walking speed in (c) the Near condition and (b) the Far condition. Note that smaller subsets S=0,3,6 (green, cyan, black) illustrate the effect of distance, as nearly all were in the near zone (5 neighbors) or the far zone (7 neighbors).

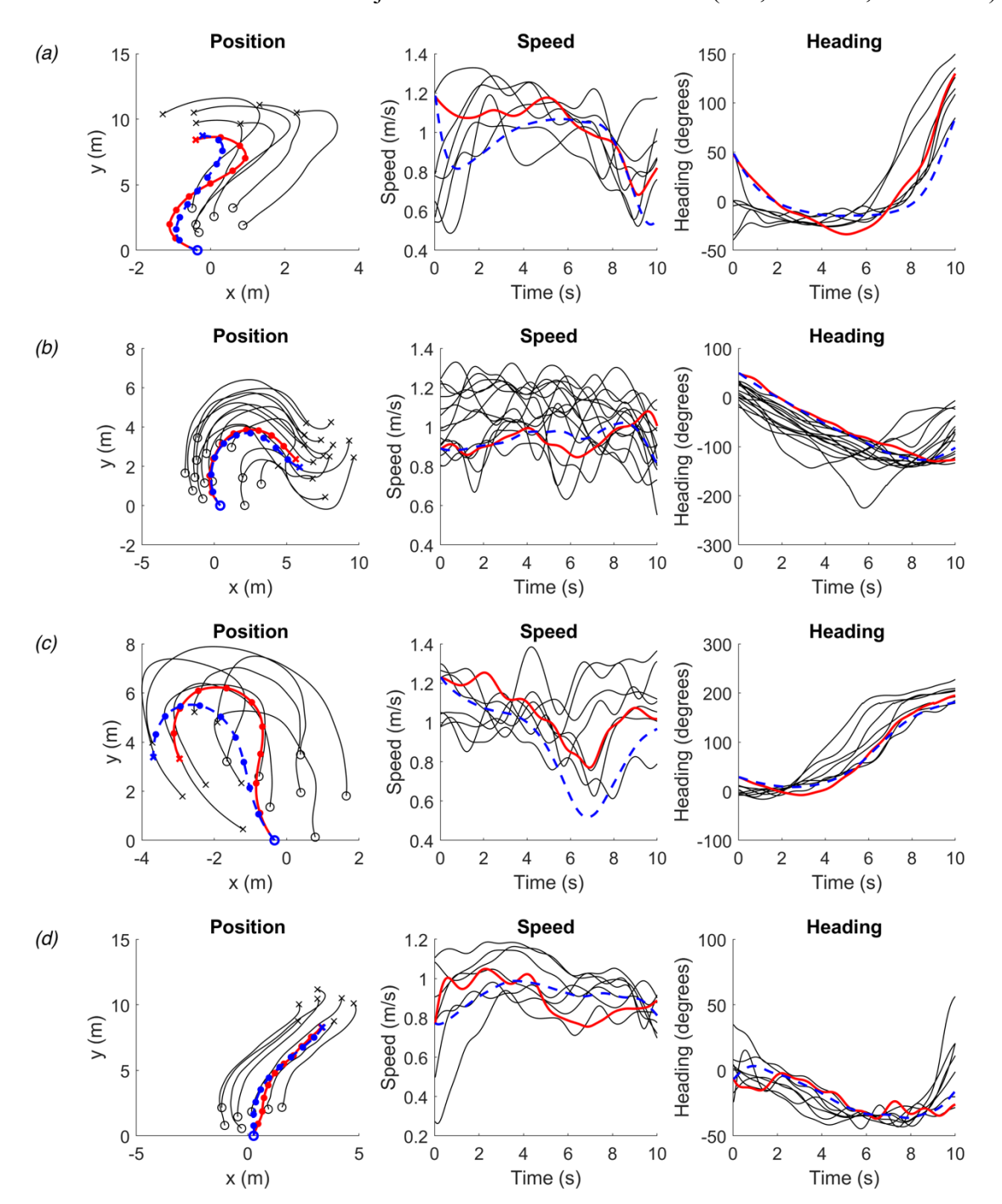


Figure S4. Simulations of sample 10s segments from the human 'swarm' data. (a) IPD=2m, mean position error=0.51m, speed r=.76 (RMSE=0.14 m/s), heading r=0.94, (RMSE=21.12°). (b) IPD=1m, mean position error=0.32m, speed r=0.24 (RMSE=0.07 m/s), heading r=0.99 (RMSE=9.3°). (c) IPD=2m, mean position error=0.60m, speed r=0.80 (RMSE=0.18m/s), heading r=0.94 (RMSE=10.01°). (d) IPD=2m, mean distance error=0.29m, speed r=0.33 (RMSE-0.11 m/s), heading r=0.86 (RMSE=7.14°). Participant = solid red curve, model = dashed blue curve, neighbors = black curves; O=starting positions, X=final positions.